Detection of General Edges and Keypoints *

L. Rosenthaler[1], *F. Heitger*[1], *O. Kübler*[1] *and R. von der Heydt*[2]

[1] Communication Technology Laboratory, ETH-Zürich, CH-8092 Zürich
Email: rosenth@vision.ethz.ch
[2] Department of Neurology, University Hospital Zürich, CH-8091 Zürich

Abstract. A computational framework for extracting (1) edges with an arbitrary profile function and (2) keypoints such as corners, vertices and terminations is presented. Using oriented filters with even and odd symmetry we combine their convolution outputs to oriented energy resulting in a unified representation of edges, lines and combinations thereof. We derive an "edge quality" measure which allows to test the validity of a general edge model. A detection scheme for keypoints is proposed based on an analysis of oriented energy channels using differential geometry.

1 Introduction

The interpretation of static, monocular grey-valued images is usually based on the hypothesis that the loci of strong intensity variation are tightly coupled to physical events such as 3D discontinuities (foreground/background) or changes of surface orientation. However, the corresponding intensity variations normally differ from ideal edges. They often have complex profiles and may not be perfectly straight. Therefore, edge detection has to be a truly 2D process and linear operators based on idealized edge-models (e.g. Canny [4]) seem to be inadequate for detecting complex intensity distributions.

Perona & Malik [16] have pointed out that, in general, linear operators cannot detect and localize correctly edges and lines simultaneously. This problem becomes relevant in real images as many "natural" edges are neither a pure edge or a line, but rather have complex intensity profiles. Second order non-linearities in the form of local energy may provide a solution to the problem [6] [1] [13] [12] [15] [16].

Yet, energy models and their "linear" precursors are intrinsically one-dimensional. They cannot account for another important class of image features: corners, vertices, terminations, junctions etc.. These two-dimensional intensity variations indicate, for example, strong variations in contour orientation, terminations occurring in occlusion situations and many other relevant 2D features.

In this paper we propose a dual processing scheme which emphasizes the detection of 1D signal variations on the one hand, and of points of strong 2D variations on the other. We present a method which allows (1) to derive a valid indicator for the presence of 1D edges with arbitrary profiles and (2) to detect and localize complex 2D intensity variations. We use the term *general edge* (GE) for regions of 1D intensity variation and the term *keypoint* for points of strong 2D intensity variation. The concept of a general edge allows to develop a fully 2D filter model based on linear filters which are polar separable in the Fourier domain. Even and odd filter outputs are then combined to oriented energy.

Two aspects of our approach are new: (a) The use of a contrast independent measure for deviations from a general edge; this enables us to limit the application of the edge model to points that qualify as general edge points. The local maxima of oriented energy

* The research described in this paper has been supported by the Swiss National Science Foundation, Grant no. 32-8968.86.

can then be used to localize the edges [16],[12]. (b) The use of differential geometry applied to oriented energy maps, yielding a representation of strong 2D intensity variations (keypoints).

The work presented here was partially motivated by our interest in biological mechanisms of contour processing [20] [19] [17] [7].

2 General Edge, Orientation Filters and Local Energy

We define general edges (GE) to be image features with an arbitrary intensity variation in one direction and constant intensity orthogonal to it. The spectrum of a GE is restricted to a central slice in Fourier space (cf. [2]). This property of GEs make orientation filters that are polar separable in the Fourier domain a natural choice because they allow to separate filter responses into a term which depends on the profile of the GE and a term that depends only on the difference between filter and edge orientation. Using polar coordinates in the frequency plane, we define the 2-D filters $F_n(\nu,\psi) = H(\nu)\Omega_n(\psi)$ where $H(\nu)$ defines the radial bandpass characteristics and Ω_n (satisfying $\Omega_n(\psi) = \Omega_n(\psi+\pi)$) controls the orientation selectivity of the filters (n: orientation index). In this paper, we use $\Omega_n(\psi) = \cos^{2p}\left(\psi - \theta_n - \frac{\pi}{2}\right)$ with θ_n defining filter orientation.

With f_n being the inverse Fourier transform of F_n the convolution with a GE of orientation θ has the form $s(x,y) * f_n(x,y) = \Omega(\theta - \theta_n) \cdot g(x,y)$. Choosing $(\hat{x},\hat{y})$ as the rotated coordinate system with $\hat{x}$ in the direction of the GE, $g(x,y)$ becomes a 1D function $g(\hat{y})$ which is the convolution of the 1D GE profile with the radial term of the filter $H(\nu)$. In other words, polar separable filters allow to split up the convolution result with a GE into a term depending on orientation and a term depending on the profile of the GE. This reduces the design of the bandpass characteristics to a 1D problem.

Since we allow GEs to have arbitrary profiles, simple linear filtering (e.g. [11] [4]) cannot warrant correct localization. Local energy concepts, however, as proposed by [6] [13] [12] [15], seem to overcome this deficit in that they unify the detection of edges, lines and hybrid forms. Local energy requires for each orientation n a pair of even and odd filters whose convolution output is combined by quadrature pair summation to form local energy. A common method is to construct these filter pairs as Hilbert transforms of each other [13] [16].

In general, however, Hilbert pairs do not guarantee a monomodal line response in local energy. Gabor pairs, as proposed by Adelson et al. [1], show a monomodal line response but have the drawback that the even Gabor does not integrate to zero. We modified the Gabor scheme by introducing a frequency sweep such that both filters integrate to zero (cf. [7]). The Fourier transform of these 1D filters provides the radial term $H(\nu)$ of the polar separable 2D filters. In the present paper, local energy is then defined as the square root of the sum of the squared response of odd and even filters.

3 Local Orientation and Contour Quality

Using a sufficient number of different orientations, it is possible to determine the exact orientation θ of a GE: Let E_j be the energy response in orientation j and E_{max} the maximum over all orientations. Now we define $Q(\psi)$ as

$$Q(\psi) = \sum_{j=0}^{N-1} \left(\frac{E_j(\mathbf{r})}{E_{max}(\mathbf{r})} - \frac{\Omega\left(|\psi - \theta_j|\right)}{\Omega\left(\min_{k=0,\ldots,N-1} |\psi - \theta_k|\right)} \right)^2 \qquad (1)$$

Since the filters are polar separable in the Fourier domain, it is possible to write $E_j = S{\cdot}\Omega\left(\theta - \theta_j\right)$ and, since Ω is a monomodal function, $E_{max} = S{\cdot}\Omega\left(\min_{k=0,\ldots,N-1} |\theta - \theta_k|\right)$. Therefore $Q(\psi) = 0 \Leftrightarrow \psi = \theta$. Finding the exact orientation θ of a GE amounts to searching for $Q_{min} = \min_{\psi=0,\pi} Q(\psi)$ with ψ_{min} being the angle where $Q(\psi) = Q_{min}$.

The value Q_{min} is a measure of GE conformity. It is zero for a GE and increases with increasing deviation from a perfect GE. If Q_{min} is greater than a threshold value Q_{th} we consider the image structure to differ significantly from a GE. We take the local orientation as given by ψ_{min}, if $Q_{min} < Q_{th}$. Otherwise a unique orientation is not defined. Fig. 1 shows in the top row four samples of a trihedral vertex with increasing levels of additive gaussian noise. The center row represents the values of Q_{min} and ψ_{min}. The orientation of the lines corresponds to ψ_{min} whereas the match with the general edge model is expressed by line length $L = (1 + Q_{min})^{-1}$. L can be considered an estimate of "GE quality". Fig. 1 clearly shows how L decreases in the neighbourhood of a vertex. Noise also leads to a degradation of L. The bottom row shows the result of edge detection given by the local maxima in energy orthogonal to the orientation ψ_{min}. Edge processing stops where the GE model is no longer valid.

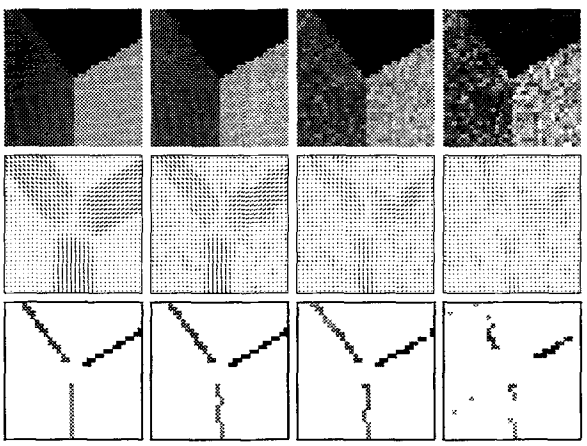

Fig. 1. Edge quality maps. The top row shows a sample vertex, corrupted by increasing levels of noise (from left to right: no noise, 20dB, 10dB and 5dB SNR). The center row shows a plot of local orientation and edge quality, and the bottom row shows the result of edge detection. The computing was done on 128x128 pixel images to avoid border effects. Shown are 32x32 pixel cuts from the central part of the images.

4 Keypoints

In the previous section we have described a method of finding GEs using a measure of quality. On the other hand, there is a class of important image features with pronounced 2D variation of intensity such as line endings, corners, junctions etc. (*keypoints*). In this section we present a method for detecting these keypoints. It is based on the oriented energy maps and does not rely on an explicit model of any particular 2D intensity distribution.

The basic idea is to exploit the fact that deviations from a GE result in changes of local energy magnitude along the edge. Deviations may be induced by all sort of image features such as (a) a loss of contrast (e.g. line ending), (b) two or more edges of different orientation meeting at one point (e.g. corner, vertex) or (c) continuous changes of orientation (curvature). Directional derivatives in the orientation of a contour seem to be a straight-forward way for detecting keypoints. Local extrema of the first directional derivatives would indicate features like line-endings, corners and junctions. For strong curvature and blobs the second directional derivatives would be more appropriate.

On general edges, the derivatives along the edge orientation are zero. At keypoints a unique orientation cannot be assigned and thus derivatives in a single orientation are inadequate for representing such features. Using the property that oriented energy separates orientational components, we propose to take for each energy channel the directional derivatives *parallel* to its orientation. We expect keypoints to have local extrema in derivative magnitudes. However, the directional derivatives are non-zero, also on GEs, for all

orientations that differ from the edge orientation. We show that these "false responses" can be selectively eliminated by a compensation scheme that makes use of the systematic nature of these errors. This compensation scheme is based on derivatives *orthogonal* to each oriented energy channel. We use the terms *p-derivative* and *o-derivative* for directional derivatives *parallel* and *orthogonal* to the orientation of a channel, respectively.

Assuming N filters with orientations given by $\theta_n = \frac{\pi n}{2}$ and a GE with orientation θ, we define $\boldsymbol{\theta}_n$ as unit vector parallel to filter orientation and $\boldsymbol{\theta}_{n_\perp}$ as unit vector orthogonal to filter orientation. At location $\mathbf{r}$ we define

$$P_n^{(1)}(\mathbf{r}) = \left|\frac{\partial E_n(\mathbf{r})}{\partial \boldsymbol{\theta}_\mathbf{n}}\right| \text{ and } P_n^{(2)}(\mathbf{r}) = \left[-\frac{\partial^2 E_n(\mathbf{r})}{\partial \boldsymbol{\theta}_\mathbf{n}{}^2}\right]^+ \text{, with } [\xi]^+ = \max(0,\xi) \qquad (2)$$

as the gradient magnitude *parallel* to filter orientation (1st p-derivative) and as an estimate of negative curvature of the magnitude of local energy along filter orientation (2nd p-derivative). The latter corresponds to 'bump's' of local energy along filter orientation. Since we are not interested in local minima along oriented energy, $P_n^{(2)}(\mathbf{r})$ is defined to be zero for positive values of the second directional derivative. Fig. 2 shows oriented energy E_n and its directional p-derivatives for a sample corner. Each column represents one orientation channel. With above definitions and in analogy to local energy we may define a scalar *keypoint map* $\hat{K}(\mathbf{r})$:

$$\hat{K}(\mathbf{r}) = \max_{n=0,N-1} \sqrt{P_n^{(1)}(\mathbf{r})^2 + P_n^{(2)}(\mathbf{r})^2}$$

In Fig. 3 the raw keypoint map $\hat{K}$ is depicted for a sample corner, a line ending and a T-junction. As mentioned above, the 1st and 2nd p-derivative will be zero on a GE only if $(\theta - \theta_n) = 0$. For $(\theta - \theta_n) \neq 0$, 1st p-derivatives will be zero only at the exact location of a GE and 2nd derivatives will always be > 0 with a local maximum on the GE. Because of these "false responses" to GEs, $\hat{K}$ is insufficient for detecting keypoints selectively. The systematic nature of these false responses allows to construct a compensation map $C(\mathbf{r})$:

$$K(\mathbf{r}) = \left[\hat{K}(\mathbf{r}) - C(\mathbf{r})\right]^+$$

Using the properties of a separable filter (orientation selectivity given by $\cos^{2p}(\theta - \theta_n)$) and the properties of GEs (the local energy of a GE is a GE too), it is easy to show the following relations:

$$P_n^{(1)}(\mathbf{r}) = s(\mathbf{r})\cos^{2p}(\theta - \theta_n)\sin(\theta - \theta_n) \quad , \quad P_n^{(2)}(\mathbf{r}) = s(\mathbf{r})\cos^{2p}(\theta - \theta_n)\sin^2(\theta - \theta_n) \qquad (3)$$

where $s(\mathbf{r})$ depends only on the profile of the GE and on the distance from its center. Eqn. (3) suggests to use the directional derivatives *orthogonal* to the filter orientation as the compensation signal for the systematic error of $\hat{K}$. In analogy to the p-derivatives we define the 1st and 2nd o-derivatives as

$$O_n^{(1)}(\mathbf{r}) = \left|\frac{\partial E_n(\mathbf{r})}{\partial \boldsymbol{\theta}_{\mathbf{n}_\perp}}\right| \text{ and } O_n^{(2)}(\mathbf{r}) = \left[-\frac{\partial^2 E_n(\mathbf{r})}{\partial \boldsymbol{\theta}_{\mathbf{n}_\perp}{}^2}\right]^+$$

On a GE, the following relation holds:

$$O_n^{(1)}(\mathbf{r}) = s(\mathbf{r})\cos^{2p+1}(\theta - \theta_n) \text{ and } O_n^{(2)}(\mathbf{r}) = s(\mathbf{r})\cos^{2p+2}(\theta - \theta_n) \qquad (4)$$

For all θ of a GE, the maxima of the 1st and 2nd o-derivatives are greater than the maxima of the 1st and 2nd p-derivatives. Therefore,

$$\sum_{k=0}^{N-1}\left(O_k^{(1)}(\mathbf{r}) + O_k^{(2)}(\mathbf{r})\right) > \sqrt{\left(P_n^{(1)}(\mathbf{r})\right)^2 + \left(P_n^{(2)}(\mathbf{r})\right)^2} \text{ , } n = 0, N-1 \text{ .}$$

Using the sum over all orientations as compensation has the advantage that it is robust in discrete implementations and we can define the compensation map as

$$\hat{C}(\mathbf{r}) = \sum_{k=1}^{N-1} \left(O_k^{(1)}(\mathbf{r}) + O_k^{(2)}(\mathbf{r}) \right) \quad \text{and} \quad K_c(\mathbf{r}) = \left[\hat{K}(\mathbf{r}) - \hat{C}(\mathbf{r}) \right]^+$$

However, $\hat{C}$ is not zero at keypoints (e.g. at a line ending) as can be seen in Fig. 3. Keypoints are characterized by the fact that the orientation distribution of local energy differs significantly from the distribution on a GE. This fact can be used to implement a correction mechanism by combining orthogonal pairs of $O_k^{(2)}(\mathbf{r})$ to form a new map $\hat{R}$:

$$\hat{R}(\mathbf{r}) = \sum_{k=0}^{N/2-1} \sqrt{O_k^{(2)}(\mathbf{r}) \cdot O_{k_\perp}^{(2)}(\mathbf{r})} \tag{5}$$

Fig. 3 shows $\hat{R}$ for the three sample keypoints. Obviously $\hat{R} > 0$ on GEs, but it remains almost constant with varying θ (substitute (4) into (5)).

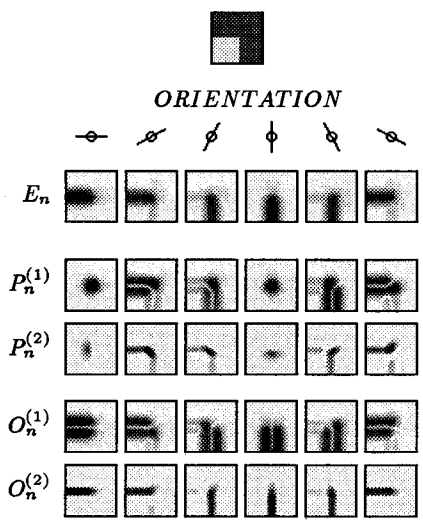

Fig. 2. Responses to a 90^0 corner (top image) of oriented energy E_n, first p-derivative $P_n^{(1)}$, second p-derivative $P_n^{(2)}$, first o-derivative $O_n^{(1)}$ and second o-derivative $O_n^{(2)}$. Image dimensions are 32×32 pixels; filter parameters are $p = 2, \sigma = 3$.

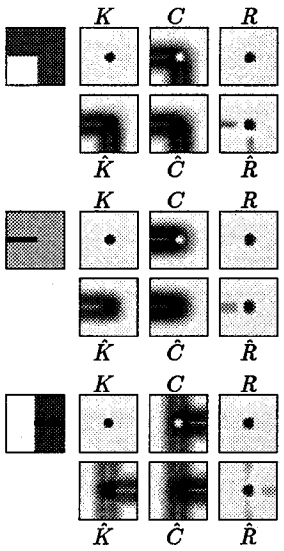

Fig. 3. Keypoint detection using a corner, a line-end and a T-junction (32x32 pixels). Top rows: original image, final keypoint map (K), corrected compensation map (C), corrected combination of o-derivatives (R). Bottom rows: uncompensated keypoint map ($\hat{K}$), raw compensation map $\hat{C}$ and uncorrected R map ($\hat{R}$).

The extrema $\hat{R}_{\max}$ and $\hat{R}_{\min}$ differ by less than 10 percent of $\hat{R}_{\max}$ (using filters with $N = 6$ and $p = 2$). It is interesting to note that, supposing that N is even and $N > (p+1)$, the sum over all 2nd o-derivatives is constant and does not depend on θ. Therefore we estimate the error of $\hat{R}(\mathbf{r})$ on GEs with the sum over all 2nd o-derivatives and define

$$R(\mathbf{r}) = \left[\sum_{k=0}^{N/2-1} \sqrt{O_k^{(2)}(\mathbf{r}) \cdot O_{k_\perp}^{(2)}(\mathbf{r})} - \gamma \cdot \sum_{k=0}^{N-1} O_k^{(2)}(\mathbf{r}) \right]^+ \tag{6}$$

An estimate of γ can be easily derived setting $\theta = 0$, substituting (4) into (6) and resolving the resulting equation for $R(\mathbf{r}) = 0$. With this definition of $R(\mathbf{r})$ we finally define the following compensation map C:

$$C(\mathbf{r}) = \sum_{k=0}^{N-1} \left(\left[O_k^{(1)}(\mathbf{r}) - R(\mathbf{r}) \right]^+ + \left[O_k^{(2)}(\mathbf{r}) - R(\mathbf{r}) \right]^+ \right)$$

This compensation map fulfills all requirements: (1) it cancels successfully all systematic errors of the raw keypoint map at general edges, and (2) it is zero at the location of keypoints. Fig. 4 shows the different steps of keypoint detection on a simple gray-valued image. The keypoint detection scheme has been tested on a wide variety of complex natural scenes. Results will be shown in the next section.

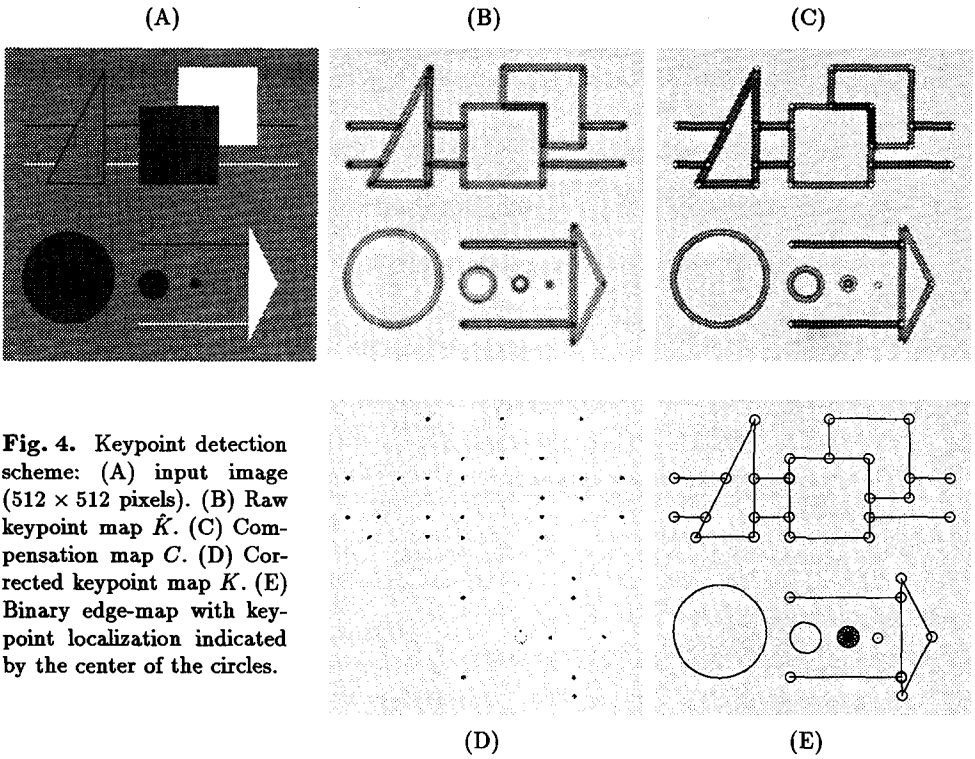

Fig. 4. Keypoint detection scheme: (A) input image (512 × 512 pixels). (B) Raw keypoint map $\hat{K}$. (C) Compensation map C. (D) Corrected keypoint map K. (E) Binary edge-map with keypoint localization indicated by the center of the circles.

5 Experimental results

Implementation: Convolutions with the twelve filter kernels were carried out in the Fourier domain. Six maps of oriented energy were generated by quadrature pair summation of even and odd filter convolution outputs (we took the squareroot of oriented energy to reduce signal dynamics to those of the original filter outputs). Binary edge maps were generated by finding local maxima orthogonal to the orientation of the best responding energy channel at each location.

To compute the derivatives in the various directions oriented energy maps were sampled at discrete offset positions around center pixels. First derivatives corresponded to the difference in value at two offset pixels and second derivatives to their average minus the value of the center pixel.

Complex scenes: We have tested our contour and keypoint detection scheme with a variety of images of different complexity. One example is shown in Fig. 5A, an outdoor scene. The scene contains primarily corners and vertices, but also some T-junctions (fence in the lower part of the image). A large proportion are occlusion features generated by the foreground object occluding structures of the building in the background. The curved shape of the sculpture thus introduces some interesting variation in termination angles. The result of the keypoint detection scheme is shown in Fig. 5B.

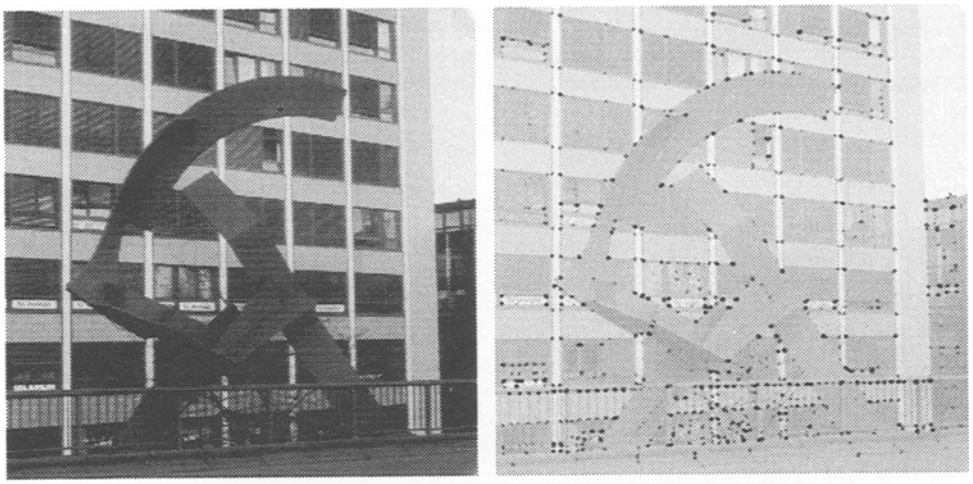

Fig. 5. Application of the keypoint scheme to an outdoor scene: (A) input image. (B) keypoint map superimposed on a contrast reduced version of the original image. Image size is 512×512 pixels and filter parameters are $p = 2$ and $\sigma = 2$.

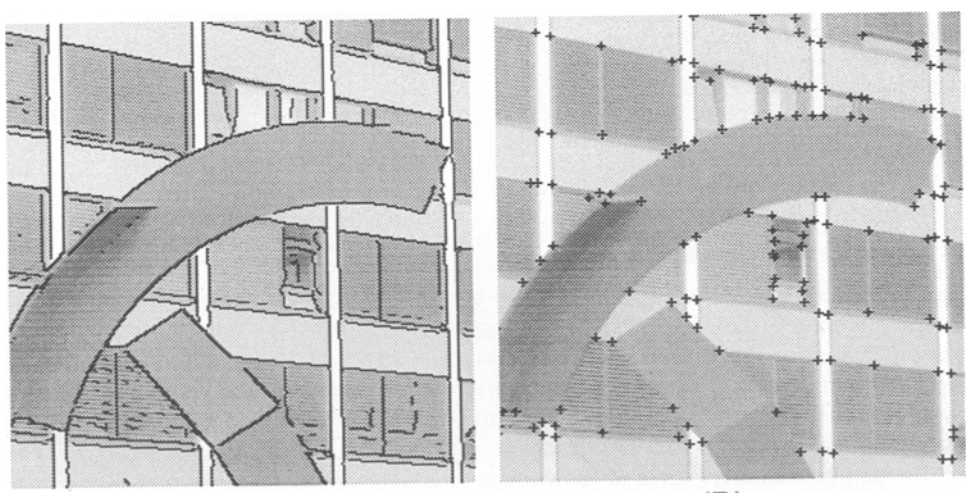

Fig. 6. Edge map (A) and keypoint localization (B) for a subsection of image in Fig. 5. Keypoint positions (pixel accuracy) are indicated by crosses.

The dark blobs correspond to the keypoint map superimposed on a contrast reduced version of the original image. Note that the keypoint strength is a function of local image contrast. Thus weaker markings do not necessarily indicate a weaker evidence for the presence of a corner, vertex etc.. It can be seen that no markings, whatsoever, occur on straight contour segments. This proves our compensation scheme to be effective also with more complex 2D intensity configurations. Fig. 6A shows, for a part of the image, the contour map extracted with the non-maximum suppression scheme described above. A threshold of 8% of the maximal oriented energy response was applied. One can see that while straight parts of contour are well represented we often find gaps or distortions in the neighbourhood of keypoints. Fig. 6B shows the location of keypoints indicated by crosses (threshold again 8% of the global keypoint maximum). As both general edge and keypoint location have been derived from oriented energy, the maps are commensurable and complementary.

6 Discussion

We have presented a computational framework for extracting (1) intensity discontinuities which can be described as 1D variations (general edges) and (2) keypoints with a true 2D intensity distribution (corners, vertices, terminations etc.).

Using oriented filters with even and odd symmetry we combine their convolution outputs to oriented energy. This quadrature pair summation has the advantage that edges and lines and combinations thereof are treated in a unified way and can be unambiguously localized [12], [15], [16]. The edge quality measure we derived is used to select for the edge map only those pixels that exceed a predefined quality. This way we can be sure edge detection is valid at these locations.

The detection scheme for keypoints represents a novel approach to the problem of detecting and localizing image features like corners, junctions or terminations. This is more difficult than detecting edges. The abundant richness of two-dimensional intensity variations seems to prohibit approaches of the form of simplified model prototypes as, for example, the Heaviside function used in edge models. What seems to be important is to reduce the dimensionality of the problem by generating invariant representations. Oriented energy is invariant with respect to the polarity and the type of edge [15].

We propose to detect keypoints by taking first and second derivatives on the energy maps in the filter direction (p-derivatives). The idea is that true 2D features produce strong variations in the energy signal parallel to its orientation. However, markings also occur for general edges if its orientation and the direction of the derivative differ. We have introduced a scalar compensation map that selectively suppresses these unwanted derivative signals.

It seems that differential geometry is an adequate way to attack two-dimensional intensity variations. However, compared to other approaches that also use methods of differential geometry (e.g. [3], [10], [5]) , our model is not gray-level based (smoothed version of the original image) but uses oriented energy maps which have the advantage of representing different edge types in a unified way. Furthermore, our approach does not contain any specific model of keypoints, as for example a corner [9], [14], [18], vertex [5], T- or L-junctions. In this respect we cannot expect selectivities for these specific 2-D intensity variations. Our scheme detects and accurately localizes corners (di-, tri-, tetra-hedral junctions of different angles and contrasts) as well as line-terminations, T-junctions, strong curvature and blobs. However, the information given by the first and second p-derivatives in different orientations may be used to classify the keypoints. We are currently working on a processing scheme to classify keypoints paying attention to occlusion situations and to the distinction between foreground/background structures.

Parallels in biological vision: Some of the ideas of the work presented here originated from our interest in the simulation of neural contour mechanisms [7]. In fact the different stages of our computational approach can be compared to stages in cortical processing of visual information: even and odd symmetrical, orientation selective filters can be compared to the properties of simple cells. The oriented energy representation is consistent with complex cells which are known to exhibit phase independence [12]. Hypercomplex or end-stopped cells respond well to short bars, line-ends and corners [8]. We have related the response behaviour of single- and double-stopped cells to first and second derivative operations based on orientation selective complex cells [7]. These endstopped-operators can be used to generate "subjective contours". The results have demonstrated the importance of detecting keypoints when dealing with the problem of spatial occlusion.

References

1. Adelson, E. H. & Bergen, J. R.: Spatio-temporal energy models for the perception of motion. Journal of the Optical Society of America A **2** (1985) 284-299
2. Barrett, H. B., & Swindell, W.: Analog Reconstruction for Transaxial Tomography. Proceeding of the IEEE **65** (1977) 89-107
3. Beaudet, P. R.: Rotationally invariant image operators. 4th International Joint Conference on Pattern Recognition, Kyoto, Japan (1978) 578-583
4. Canny, J.: A computational approach to edge detection. IEEE Transactions on Pattern Analysis and Machine Intelligence **8** (1986) 679-698
5. Giraudon, G. & Deriche, R.: On corner and vertex detection. IEEE Proc. CVPR'91, Maui, Hawai (1991) 650-655
6. Granlund, G. H.: In search of a general picture processing operator. Computer Graphics and Image Processing **8** (1978) 155-173
7. Heitger, F., Rosenthaler, L., von der Heydt, R. Peterhans, E. and Kübler, O.: Simulation of neural contour mechanisms: From simple to end-stopped cells. Vision Research **32** (1992) in press
8. Hubel, D. H. & Wiesel, T. N.: Receptive fields and functional architecture of monkey striate cortex. Journal of Physiology, London **195** (1968) 215-243
9. Kitchen, L. & Rosenfeld, A.: Gray level corner detection. Pattern Recognition Letters **1** (1982) 95-102
10. Koenderink, J. J. & van Doorn, A. J.: Representation of local geometry in the visual system. Biological Cybernetics **55** (1987) 367-376
11. Marr, D. & Hildreth, E.: Theory of edge detection. Proceedings of the Royal Society, London Series B **207** (1980) 181-217
12. Morrone, M. C. & Burr, D. C.: Feature detection in human vision: A phase-dependent energy model. Proceedings of the Royal Society, London Series B **235** (1988) 221-245
13. Morrone, M. C. & Owens, R. A.: Feature detection from local energy. Pattern Recognition Letters **6** (1987) 303-313
14. Noble, J. A.: Finding corners. Image Vision and Computing **6** (1988) 121-128
15. Owens, R., Venkatesh, S. & Ross, J.: Edge detection is a projection. Pattern Recognition Letters **9** (1989) 233-244
16. Perona, P. & Malik, J.: Detecting and localizing edges composed of steps, peaks and roofs. UCB Technical Report, UCB/CSD90/590 (1990)
17. Peterhans, E. & von der Heydt, R.: Mechanisms of contour perception in monkey visual cortex. II. Contours bridging gaps. Journal of Neuroscience **9** (1989) 1749-1763
18. Rangarajan, M., Shah & Brackle, D. V.: Optimal corner detector. Computer Vision Graphics and Image Processing **48** (1989) 230-245
19. von der Heydt, R. & Peterhans, E.: Mechanisms of contour perception in monkey visual cortex. I. Lines of pattern discontinuity. Journal of Neuroscience **9** (1989) 1731-1748
20. von der Heydt, R., Peterhans, E. & Baumgartner, G.: Illusory contours and cortical neuron responses. Science **224** (1984) 1260-1262